2

NASA TECHNICAL MEMORANDUM

NASA TM X- 71572

NASA TM X-71572

STUDY OF LUBRICANT JET FLOW PHENOMENA IN SPUR GEARS

by L. S. Akin, D. P. Townsend,
and J. J. Mross
Lewis Research Center
Cleveland, Ohio

TECHNICAL PAPER proposed for presentation at
Lubrication Conference sponsored by the American
Society of Mechanical Engineers and the American
Society of Lubrication Engineers
Montreal, Canada, October 8-10, 1974

2

STUDY OF LUBRICANT JET FLOW PHENOMENA IN SPUR GEARS

by L.S. Akin,* D.P. Townsend,** and J.J. Mross*
Lewis Research Center
National Aeronautics and Space Administration
Cleveland, Ohio 44135

E-8012

ABSTRACT

Lubricant jet flow impingement and penetration depth into a gear tooth space were measured at 4920 and 2560 RPM using a 8.89 cm (3.5 inch) pitch diameter 8 pitch spur gear at oil pressures from 7×10^4 to 41×10^4 N/m^2 (10 psi to 60 psi). A high speed motion picture camera was used with xenon and high speed stroboscopic lights to slow down and stop the motion of the oil jet so that the impingement depth could be determined. An analytical model was developed for the vectorial impingement depth and for the impingement depth with tooth space windage effects included. The windage effects on the oil jet were small for oil drop size greater than .0076 cm (.003 inches). The analytical impingement depth compared favorably with experimental results above an oil jet pressure of 7×10^4 N/m^2 (10 psi). Some of this oil jet penetrates further into the tooth space after impingement. Much of this post impingement oil is thrown out of the tooth space without further contacting the gear teeth.

---

*General Electric Co., Marine Turbine and Gear Products, Member ASME
**NASA-Lewis Research Center, Member ASME

NOMENCLATURE

$\overline{A}$	Horizontal tooth space distance from impingement point, m(inches)
a_t	Tangential acceleration, m/sec^2 (ft/sec^2)
a_r	Radial acceleration, m/sec^2 (ft/sec^2)
B	Backlash of gear set P_d m(inches)
$\overline{B}$	Horizontal tooth space distance to impingement point, m(inches)
C_d	Drag coefficient for air
d	Pitch diameter of gear, m(inches)
d_o	Diameter of oil droplet, m(inches)
$F_{x,y,z}$	Forces in x, y and z direction, N(lb)
g	Acceleration due to gravity, m/sec^2 (ft/sec^2)
H	Measured impingement depth, m(inches)
H_v	Vectorial impingement depth, m(inches)
H_w	Windage impingement depth, m(inches)
H'_v	Approximate vectorial impingement depth, m(inches)
N	Number of teeth
n	Rotational speed, RPM
Δp	Differential pressure between oil and ambient, N/m^2 (psi)
Δp_h	Differential pressure for pitch line depth, N/m^2 (psi)
Δp_w	Differential pressure for working depth, N/m^2 (psi)
P_d	Diametral pitch
R_o	Outside radius of gear, m(inches)
r	Pitch radius of gear, m(inches)
t	Time relative to a, sec

t'	Time relative to b, sec
t_w	Time of flight from a to H_w, sec
v	Resultant jet velocity, m/sec (ft/sec)
v_e	Eddy current velocity, m/sec (ft/sec)
v_g	Gear velocity, m/sec (ft/sec)
v_j	Oil jet velocity, m/sec (ft/sec)
v_p	Gear pitch line velocity, m/sec (ft/sec)
v_r	Radial velocity, m/sec (ft/sec)
v_t	Tangential tooth space droplet windage velocity, m/sec (ft/sec)
v'_t	Tangential boundary layer droplet windage velocity, m/sec (ft/sec)
x_t, y_t	Coordinates of droplet, m(inches)
x_w, y_w	Coordinates of droplet at impingement, m(inches)
β	Vectorial angle of droplet, degrees
β_o	Vectorial angle of droplet at R_o, degrees
γ	Weight density N/m^3 (lb/ft^3)
δ_m	Maximum boundary layer thickness, m(inches)
θ	Impingement angle, degrees
ρ_a	Density of air, $kilogram/m^3$ ($slugs/ft^3$)
ρ_o	Density of oil, $kilogram/m^3$ ($slugs^2/ft^3$)
ϕ	Gear tooth pressure angle, degrees
ω	Angular velocity of gear, radians/sec

INTRODUCTION

The design of gear sets depends on at least three separate failure criteria. These are bending fatigue, surface fatigue or pitting, and lubrication failure or breakdown. Of these failure criteria, the least understood is the failure of the gears due to improper lubrication and cooling. The best known criteria for evaluating the lubrication failure mode is to analyze the probability of the gear drive experiencing scoring or scuffing [1]. This failure mode is associated with the breakdown of elastohydrodynamic and boundary lubricant films on the gear tooth surface [2]. The temperature of the gear tooth surfaces has an important if not controlling effect upon this phenomenon. Hence, cooling of gears must be accomplished without allowing excessive surface temperature to initiate the scoring mode of failure. Another very important aspect of the cooling phenomena in gears is that it is a controlling factor in determining the mismatch in parallelism between wide faced high-speed,high horsepower double helical drives. These drives are usually found in large marine and industrial power plant applications.

As a first step in understanding the cooling phenomena in gears, it is important to understand how oil penetrates into the gear tooth spaces under dynamic conditions. This is necessary in order to determine how much of the impinging oil is involved in the cooling and lubrication processes and how much of the lubricant is "flung-off". In addition, it is important for the design engineer to be able to specify a sufficient

oil jet pressure to assure adequate oil jet penetration into the root region of the gear teeth. The oil jet "impingement depth" is the point where the lubricant jet collides with the gear tooth while the "penetration depth" is the maximum depth of lubricant penetration after impingement. The penetration depth is usually larger than the impingement depth. An analytical model, enabling the engineer to make this determination, was developed by McCain and Alsandor [3] for a high-speed Ryder gear tester. The analysis was not verified experimentally. Further, [3] does not include the effects of windage which may be an important factor in the penetration of the jet of oil into the tooth root region.

It was indicated in [4] that the oil jet after impingement with the gear tooth surface splits up into two streams, one of which goes further down the tooth surface. If this were true, then adequate cooling could have been obtained with lower oil jet pressure than that needed for full impingement to the tooth root.

The objectives of the research reported herein is to (1) develop a kinematic tooth space entry model of a jet of oil through gear teeth and (2) compare the analytical model with experiment test results. In order to accomplish these objectives, experimental work was performed to study the penetration and "fling off" of a jet of oil entering gear teeth using high-speed photography. Gear speed and oil jet pressure were varied. An analytical model was developed considering the trajectory of an oil jet into a dynamic gear set, considering windage effects.

APPARATUS, SPECIMENS, AND PROCEDURES

Test Apparatus

The lubricant fling off tests were performed in the NASA-Lewis Research Center gear test apparatus shown in Fig. 1 and described more fully in [5]. This test rig uses the four-square principle of loading the test gears. Load is applied to the gears by a hydraulic loading system.

The test gears were 8 diametrial pitch, having a 8.89-cm (3.5-inches) pitch diameter, a 20 degree contact angle and a whole depth of 0.762 cm (0.300 inches). The gears were made with a very wide face width to allow for the coverage of light and oil spray for test conditions. The gear material was a low carbon steel.

A specially designed test gear cover was made for the fling off tests. The cover has two windows 90-degrees apart for admitting light to the test gears and a viewing window in front of the gears for viewing or photographing the fling-off phenomenon. The viewing window and light windows are protected from oil splash by shielding. These windows are constantly swept by a thin film of high velocity air blown across the windows to keep them free of oil for good light passage. V-jet, oil nozzles are located behind each of the light windows and spray a thin fan shaped stream of oil onto the gear teeth parallel to the gear axis. The nozzle used for these tests had an 80° spray angle and a 0.11 cm (0.043 in) diameter orifice. In all test conditions the oil jet was either a continuous stream or large droplets.

A large direct current power supply provides power for the one thousand watt xenon lamp used to illuminate the lubricant. The light from the zenon lamp is passed through a condenser lense to give a parallel light, it then passes through a cylindrical lense to bring the light into focus as a narrow slit of light. The light, which is reflected by a 45-degree mirror, passes through the light window and crosses the fan shaped oil stream at 90^{o}.

The lubricant used in the tests was a clear mineral oil to which was added approximately ten percent by volume of white lithopone pigment to give it the appearance of milk. When the narrow band of intense light crossed the fan of oil containing the white pigment a bright line of oil was illuminated so that it could be photographed with a high-speed camera.

A high-speed air cooled stroboscopic light is placed close to the window to light up the gear teeth so that the position of the oil jet can be determined in relation to the gear teeth. The stroboscopic system has a timer that prevents burn out of the flash tube.

A high-speed Hycam movie camera was used to photograph the oil film through a 45-degree mirror and the gear box cover window.

Test Procedure

The test lubricant was first used as a plain lubricant but as more light was required for the high-speed movie film, a method was needed to improve the lighting of the oil jet with the xenon lamp. It was decided after some investigation to use a white pigament

of very fine particles in the lubricant to reflect the light. The lubricant was then mixed with the white pigment and put into the lubrication tank and kept in circulation during each test to prevent settling.

The xenon lamp was started and the maximum power setting obtained to give maximum light. The condenser lense and the cylindrical lense were then positioned to focus the xenon light into a very high intenisty narrow beam of light about .8 mm (.032 inch) thick and 3.8 cm (1.5 inches) wide at the gear tooth top land surface.

Several tests were run at different test conditions. The gear speeds were 4920 and 2560 rpm. The camera was run at a speed that would synchronize with each gear tooth space and then at one half and one fourth the tooth synchronized speed. The lower camera speeds were run to give more light per frame for the film. This gave film speeds of 2300, 1150, and 575 frames per second for the 4920 rpm tests and 1150, 575 and 287 frames per second for the 2560 rpm tests. The oil jet pressure was varied for each speed from 7×10^4 to 41×10^4 N/m^2 (10 psi to 60 psi) to give various oil jet impingement depths into the gear tooth space.

With the xenon lamp on, the gear speed set and oil jet pressure set, the high-speed camera was started and allowed to attain the desired speed. When the camera had attained the set speed, the high-speed stroboscope was turned on for one half second at the high speeds and for one second at the lower speeds.

The film was developed and individual frames printed that would show the position of the illuminated oil at the various test conditions.

From these individual frames and the moving film strips, the depth of oil jet penetration into the gear tooth space was determined. Also, the way the oil jet was affected by the moving gear tooth was observed to determine what happened to the oil film on the gear teeth during impingement.

Analytical Approach

Tracing the locus of the trajectory of a droplet of the cooling-oil through a moving gear tooth space is a very complex task. Generally, the oil-jet trajectory will have the appearance as shown in Fig. 2 relative to a stationary nozzle and as shown in Fig. 3 relative to the gear. It is assumed in this paper that the oil-jet nozzle is directed radially inward and toward gear center. A nozzle directed otherwise in a specific practical application is applicable only in terms of a velocity component in the radial direction. The oil-jet will continue on its path from the nozzle until it encounters the windage boundary layer and subsequently enters the tooth space as shown in Fig. 3.

It will be noticed that the oil jet ligaments and droplets are turned slightly by the boundary layer velocity component v_t'. The velocity profile of the windage boundary layer is shown in Fig. 4. The separation line tilts into the tooth space at an angle of approximately 15° [6]. All of the air in the tooth space, below the separation line, and past the tooth top land trailing edge "a", is assumed to be moving at the gear pitch

line velocity v_g. The jet (or droplets) will continue to gain an increased windage velocity component v_t as it progresses toward the root diameter of the gear and collides with the tooth profile at x_w (and angle β at depth H_w, Fig. 2) or misses the tooth entirely and passes out of the tooth space at angle β_o. Obviously, angle β must be smaller than β_o or the oil jet fails to cool the tooth profile and gear cooling is restricted primarily to the top land $\overline{ab}$ as shown in Fig. 3 (where the jet is moving relative to the gear).

The chance of the lubricant droplets missing the tooth profile entirely are likely only at very shallow depths of penetration and when the droplet sizes are extremely small (say below 1 mil in equivalent diameter). Thus, as will be shown, tooth space windage may be an important consideration in determining the jet impingement depth H_w when the jet spray is highly atomized or inadequate supply pressure is provided.

It is necessary to have a logical reference point to define as time zero ($t = 0$) in order to systemize the analysis of this problem. The trailing edge of the top land (point "a" in Fig. 4) has been so selected. This topic will be much further developed in the section on "effects of tooth space windage" on impingement.

The remainder of the analysis will concentrate primarily on the effects of "space windage" on the depth of impingement required to determine the extent of cooling surface that can be provided to the cooling-oil in specific applications.

Eddy currents within the tooth space (as shown in Fig. 4) can exist. However, since it is anticipated that the velocities v_e of these eddies are relatively small, development of a model will not be considered herein. "End windage", shown in Fig. 5, is where the gear teeth act as an axial-radial flow fan. This effect coupled with helix angle effects can in extreme cases, be very important. However, this effect is not within the scope of the present analysis.

Depth of Impingement Without Windage

Fig. 6 is a schematic of a vectorial model for oil jet penetration without windage. From this figure,

$$\overline{A} = H_v \tan\phi \tag{1}$$

$$\overline{B} = H_v \cot\theta = \frac{H_v}{\tan\theta} \tag{2}$$

and $$\overline{A} + \overline{B} = \frac{1}{P_d}\left(\frac{\pi}{2} + 2\tan\phi + \frac{B}{2}\right) = H_v\left(\tan\phi + \frac{v_g}{v_j}\right) \tag{3}$$

where

$$v_g \triangleq v_p = \omega r = \frac{2\pi n}{60}\frac{d}{2(12)} \tag{4}$$

From the Bernoulli equation

$$\frac{v_j^2}{2g} + 0 = 0 + \frac{\Delta p}{\gamma} \text{ so that}$$

$$v_j = \sqrt{\frac{2g}{\gamma}\Delta p} = 13\sqrt{\Delta p} \text{ ft/sec} \quad (\Delta p \text{ in PSIG}), \tag{5}$$

Combining equations (4) and (5),

$$\frac{v_g}{v_j} = \frac{nd}{2977\sqrt{\Delta p}} = \frac{v_g}{v_p} \tag{6}$$

The velocity of approach before impingement is

$$V = \sqrt{v_j^2 + v_g^2} \quad \text{ft/sec} \tag{7}$$

The depth of impingement can now be formulated from Eq. (3):

$$H_v = \frac{1.5708 + 2\tan\phi + B/2}{P_d \left(\frac{nd}{2977\sqrt{\Delta p}} + \tan\phi \right)} \tag{8}$$

when $\phi = 20^\circ$ and $B = .060$ (@ 1 P_d)

$$H_v = \frac{2.33}{P_d \left(\frac{nd}{2977\sqrt{\Delta p}} + .364 \right)} \tag{9}$$

or as a good approximation at $\phi = 20^\circ$ and neglecting the pressure angle in denominator for large high speed gears:

$$H_v' \simeq \frac{2.33\ (2977)\ \sqrt{\Delta p}}{(P_d d)\ n} \doteq \frac{6900\ \sqrt{\Delta p}}{n\ \ N} \tag{10}$$

where: N = number of teeth = $P_d d$

If the desired H_v is known, then the required Δp can be found by returning to the original expression eq. (1) above for $\overline{A} + \overline{B}$ so that:

$$\frac{\pi}{2} + 2\tan\phi + B/2 = P_d H_v \left(\tan\phi + \frac{nd}{2977\sqrt{\Delta p}} \right)$$

and

$$\Delta p = \left[\frac{H_v P_d \ nd}{2977 \left[\frac{\pi}{2} + \frac{B}{2} + (2 - H_v P_d) \tan\phi \right]} \right]^2 \tag{11}$$

It should be noted that when

$\left(2 \leq H_v P_d \leq 2 + \frac{B}{2\tan\phi}\right) \simeq$ "working depth" at 1 P_d, so that if

the backlash B is neglected:

$$\Delta p_w \propto \left[\frac{2nd}{2977\left(\frac{\pi}{2}\right)} \right]^2 = \frac{(nd)^2}{5.466} \times 10^{-6} \qquad (12)$$

and when $\left(1 \leq H_v P_d \leq 1 + \frac{B}{2\tan\phi}\right) \simeq$ depth to pitch line at 1 P_d, likewise:

$$\Delta p_h \simeq \left[\frac{nd}{2977\left(\frac{\pi}{2} + \tan\phi\right)} \right]^2 \qquad (13)$$

and so by accepting the approximation of eq. (13) for 20° pressure angle gears:

$$\Delta p_h \simeq \left(\frac{nd}{5760} \right)^2 = \frac{(nd)^2}{33.2} \times 10^{-6} \qquad (14)$$

In subsequent sections this impingement depth will be named "vectorial depth" (H_v) in order to distinguish it from the "windage depth" (H_w). As will be shown also in subsequent sections equation (8) for H_v should be considered a good formula to use at the preliminary design stage to determine the performance of an oil-jet being supplied at a known oil pressure Δp. When the desired impingement depth H_v is specified and the nozzle pressure required to obtain the vectorial impingement depth is desired, equation (11) can be used to calculate the required Δp.

Effects of Tooth Space Windage

Considering the motion of the oil droplets with respect to windage in the tooth space in Fig. 6 requires the following fundamental equations describing the kinetics of the problem.

$$\Sigma F_x = C_d \frac{\pi}{4} d_o^2 \rho_a \frac{(V_g - V_t)^2}{2} - \rho_o \frac{\pi d_o^3}{6} a_t = 0 \quad (15)$$

$$\Sigma F_y = C_d \frac{\pi}{4} d_o^2 \rho_a \frac{v_r^2}{2} + \rho_o \frac{\pi d_o^3}{6} a_r = 0 \quad (16)$$

It is assumed that ΣF_z can be neglected in spur gears as a second order effect.

Equation (15) and (16) are solved for x_t and y_t, in terms of of the time of flight t to impingement. The point of impingement of the oil drop trajectory and the tooth profile are computed by determining the time it takes for the approaching gear tooth to catch the droplet trajectory in the x direction when the coordinates for the gear tooth and the oil drop trajectory in the y direction are coincident. The resulting time equation is:

$$\frac{\alpha}{2P_d} (\pi + \beta + 4\tan\phi) = \tan\phi \ell n(1+v_j \alpha t_w) + \ell n(1+v_g \alpha t_w) \quad (17)$$

where: $\alpha = \frac{3}{4} \frac{C_d}{d_o} \frac{\rho_a}{\rho_o}$ from equations (15) and (16) (18)

It will be noted that the time of flight t_w at impingement x_w, y_w cannot be solved explicity, but must be solved implicity using an iteration process. A mathematical series approximation to equation (17) can be provided to determine the approximate time of flight.

Subsequent to solving equation (17) the coordinages of the impingement point x_w, y_w are provided in equation (19) and (20) below.

$$x_w = v_g t_w - \frac{1}{\alpha} \ell n(1+v_g \alpha t_w) \quad (19)$$

$$y_w = \frac{1}{\alpha} \ell n(v_j \alpha t_w + 1) \quad (20)$$

Equations (19) and (20) can be used to calculate the coordinate trajectory by substituting t in place of t_w thus arriving at the coordinates y_t and x_t. It should be clear that for the sake of simplification that this model deals with a rack tooth profile instead of an actual involute gear. This will usually not cause a significant error in the coordinants of a droplet trajectory, especially for large gears. For small gears it becomes very necessary to calculate the actual depth from the top of the tooth H_w taking the circular motion of the outside diameter of the gear or pinion into account. This can be accomplished from Fig. 2 as follows:

$$H_w = R_o - [(R_o - y_w)^2 + x_w^2]^{\frac{1}{2}} \tag{21}$$

When equation (21) provides a zero or negative answer the droplet has obviously missed the tooth profile.

RESULTS AND DISCUSSION

Analytical Results

Using equation (21), the depth of impingement H_w into the gear tooth space as a function of speed is shown in Fig. 7. Since the gear used for the calculations has a small radius, the effect of speed is more severe than it would be in a very large gear. The calculations for Fig. 7 were performed using a .0076 mm (3 mil) drop size (d_o) as a result, windage for this size drop would have a very small effect on the depth of impingement for the analytical results shown in Fig. 8.

Fig. 8 shows the effect of drop size on the windage impingement depth H_w. The 10,000 RPM speed was selected so that two curves could be plotted at three different pressures farther apart than at the slower speeds. The depth of impingement has been plotted as a dimensionless parameter H_w/H_v so that the figure represents the effect of drop size on the deviation from the vectorial model. It will be noticed that there is very little effect for drop sizes larger than about .0076 cm (.003 inches). At drop sizes below about .0013 cm (.5 mil) the effect of drop size becomes very drastic at any pressure. The same general effect occurs at all speeds.

Fig. 9 is the droplet trajectory plotted along the depth y_t and pitch line distance x_t for various gear speeds. A fixed jet nozzle pressure of 14×10^4 N/m^2 (20 psi) has been selected for these calculations. This pressure provides realistic results at all four speeds for the gear size considered. Figs. 7 and 9 help emphasize the necessity of having adequate nozzle supply pressure commensurate with the speed of operation to provide the maximum amount of cooling possible for the gear size under consideration.

Experimental Results

Fig. 11 shows oil jet penetration into the tooth space at 4920 RPM, 18.6×10^4 N/m^2 (27 psi) nozzle pressure and 575 frames/sec using the xenon and stroboscopic lights. Fig. 11a shows the beginning of oil jet penetration into the tooth space. The effects of windage on the oil jet stream can be seen bending it to the right in the

direction of rotation. Fig. 11b shows the oil jet at impingement with the gear tooth. This figure shows a close agreement with the theoretical impingement depth lower boundary shown in Fig. 6. This figure also shows the jet being broken up due to windage.

Fig. 12 illustrates the total penetration of the oil particles before and after tooth impingement. Fig. 12b was photographed with the xenon lamp at 2560 RPM 13×10^4 N/m^2 (19 psi) and 1200 frames/sec. This figure shows the impingement depth and post impingement trajectory of the oil particles further into the tooth space. These post impingement particles are much smaller. A large percentage of these particles are carried out of the tooth space without further contact with the teeth thereby providing some lubrication but very little cooling. Fig 12awhich was photographed at 4920 RPM 14×10^4 N/m^2 (20 psi) nozzle pressure and 100 frames/sec. shows the post impingement trajectory more clearly.

Fig. 13 was photographed at 2560 RPM, 9×10^4 N/m^2 (13 psi) with the xenon and storobscopic lamps. Fig. 13a shows the oil jet penetrating into tooth space prior to impingement. It also illustrates the absence of windage effects on the jet stream such as bending and breaking up of the oil jet. Fig. 13b illustrates what happens to the oil jet just at tooth impingement. The oil is seen breaking up in small particles as it bounces off the tooth surface. This refutes the hypothesis of continuous flow to the tooth root according to the Schach model [7]. This model [7] and [4] say that in all cases the oil divides into two streams, one of which flows along the tooth surface to the root.

Comparison of Experimental and Analytical Results

Fig. 10 is a plot of calculated and experimental impingement depth versus jet nozzle pressure for gear speeds of 2560 RPM and 4920 RPM. At both speeds there is good agreement between the calculated and experimental impingement depths at the higher pressures. However, at the lower pressures, there is considerable difference between the calculated and experimental impingement depths. Most of this difference in impingement depth is due to viscous losses in the nozzle with the very viscous oil used. A small loss is due to windage effects not considered in this paper.

SUMMARY

Lubrication tests were conducted in the NASA-Lewis Research Center gear test apparatus modified for high speed photography of gear tooth lubrication. Oil jet lubrication was photographed with a high speed motion picture camera at gear speed of 4920 and 2560 RPM and oil jet pressures from 7×10^4 to 41×10^4 N/m^2 (10 psi to 60 psi). The oil jet was illuminated with a 1000 watt xenon lamp and the gear teeth were illuminated with a high speed stroboscopic light so that oil jet impingement depth could be determined from the film. An analytical model which included windage effects was developed and the experimental results compared with the analytical model.

The following results were obtained.

1. The analytical model provides good agreement with the experimental impingement depth.

2. Small drops of oil (less than .0076 mm (.003 inches)) will be affected by gear windage. For this reason best lubrication is provided when the oil jet is not atomized.

3. The nozzle pressure must be at least 7×10^4 N/m^2 (10 psi) to get good impingement depth predicted by the analytical model.

4. At low oil jet pressures, penetration into the tooth space is only slightly greater than the impingement depth. However, much of this oil is thrown out of the tooth space without further contacting the gear tooth profiles. Thus, most of the cooling function is accomplished above the impingement point.

ACKNOWLEDGEMENT

The authors wish to express their appreciation of the valuable assistance provided by Messrs. Ernie D. Walker and David J. Clinton, Photography Branch, NASA Lewis Research Center, Cleveland, Ohio and Mr. Wayne H. Bookmiller of General Electric Co., Lynn, Massachusetts.

References

1. Akin, LS, "An Interdisciplinary Lubrication Theory for Gears (with particular emphasis on scoring mode of failure)" Page 1178 - 95 ASME Transactions - Journal of Engineering for Industry Volume 95, Series B. No. 4, November 1973.
2. Akin, LS, "EHD Lubricant Film Thickness Formulas for Power Transmission Gears" ASME Paper 73-Lub-21 presented at the ASME-ASLE Joint Lubrication Conference, Atlanta, GA October 1973.
3. McCain JW and Alsandor E. "Analytical Aspects of Gear Lubrication on the Disengaging Side" ASLE Transactions 9, Page 202 - 211 (1966).
4. DeWinter, A and Blok, H. "Fling-Off Cooling of Gear Teeth" ASME Transactions - Journal of Engineering for Industry, Volume 95, Series B No. 5, February 1974
5. Townsend, DP and Zaretsky EV, "A Life Study of AISI M-50and Super Nitralloy Spur Gears with and without Tip Relief" ASME Paper 73-Lub-38 presented at the ASME-ASLE Joint Lubrication Conference Atlanta, Georgia, October 1973
6. Albertson, ML, Jensen, RA and Rause, H, "Diffusion of Submerged Jets" Transactions ASCE Vol. 115, 1950, page 662.
7. Schach, W. "Umlenkung eines freien Flussigkeitsstrahles an einer ebenen Platte" (Branching of a free liquid jet on a plane plate), I ngenieuv-Archiv, 5(4) page 245-265

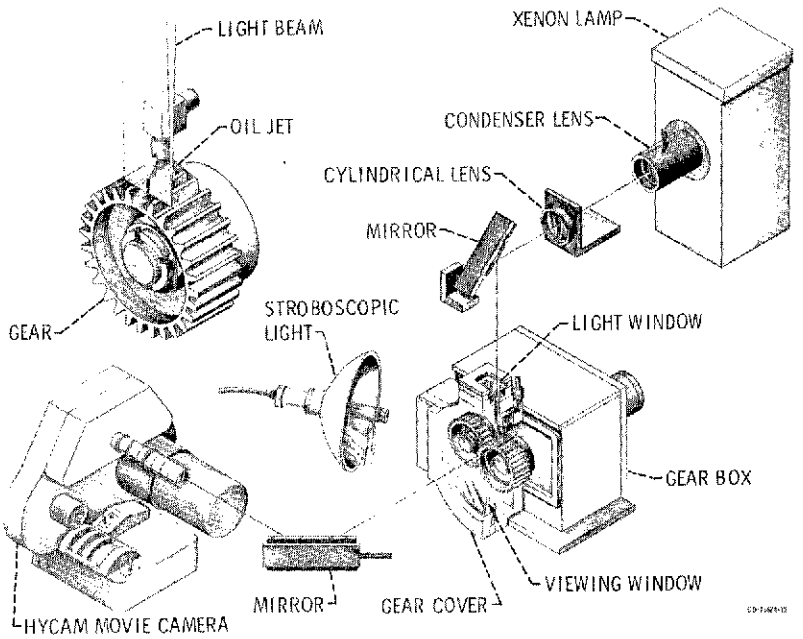

Figure 1. - Test setup for oil jet penetration study.

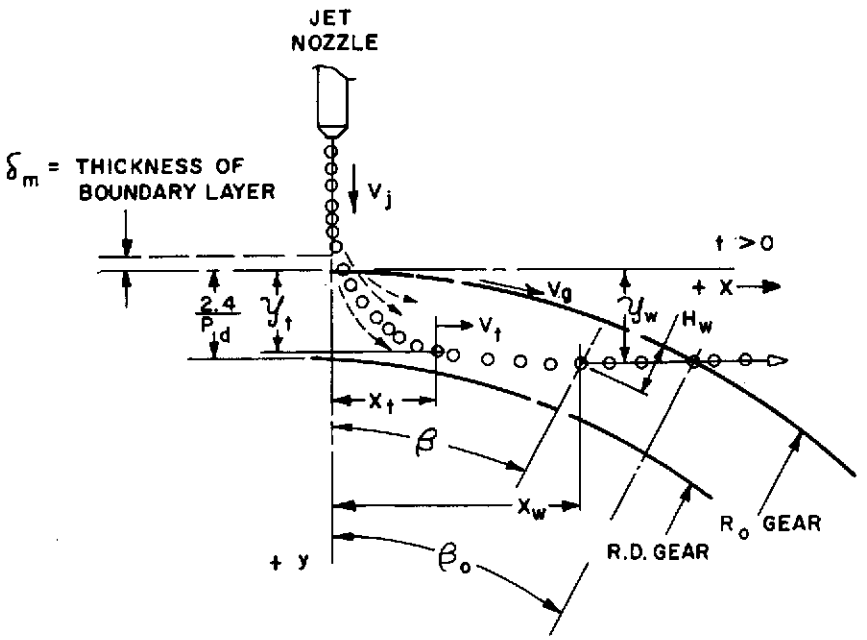

Figure 2. - Gear tooth moving past stationary jet.

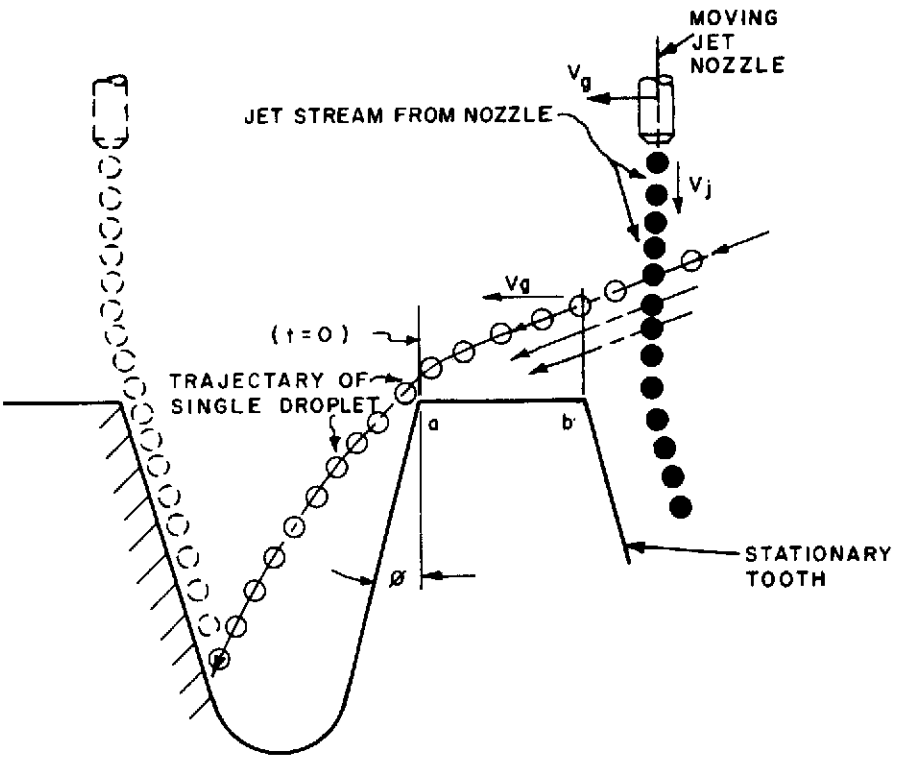

Figure 3. - Inverted motion - jet moving past stationary gear tooth.

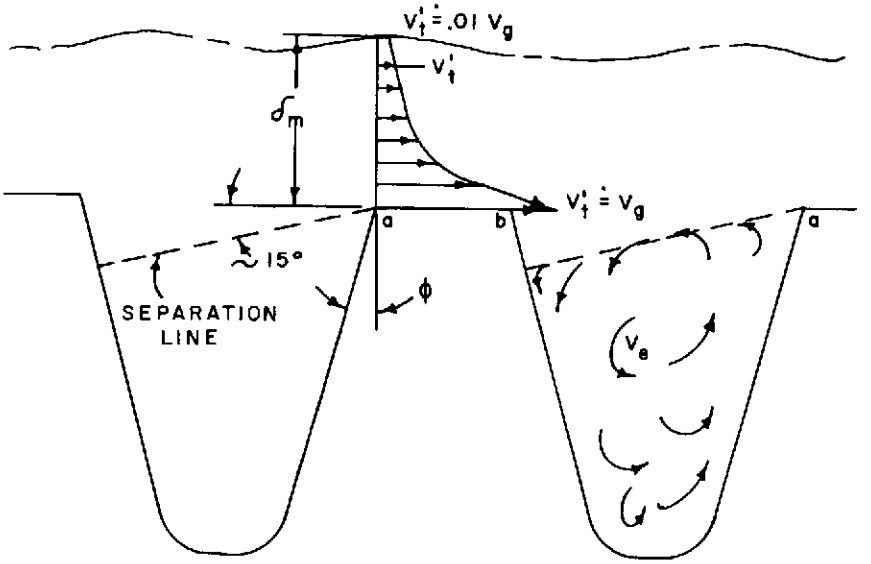

Figure 4. - Boundry layer velocity profile and eddy windage.

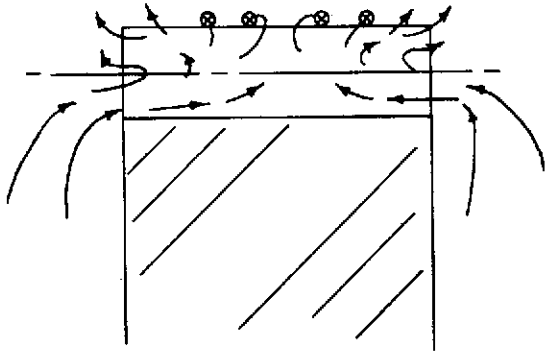

Figure 5. - Tooth end windage effect.

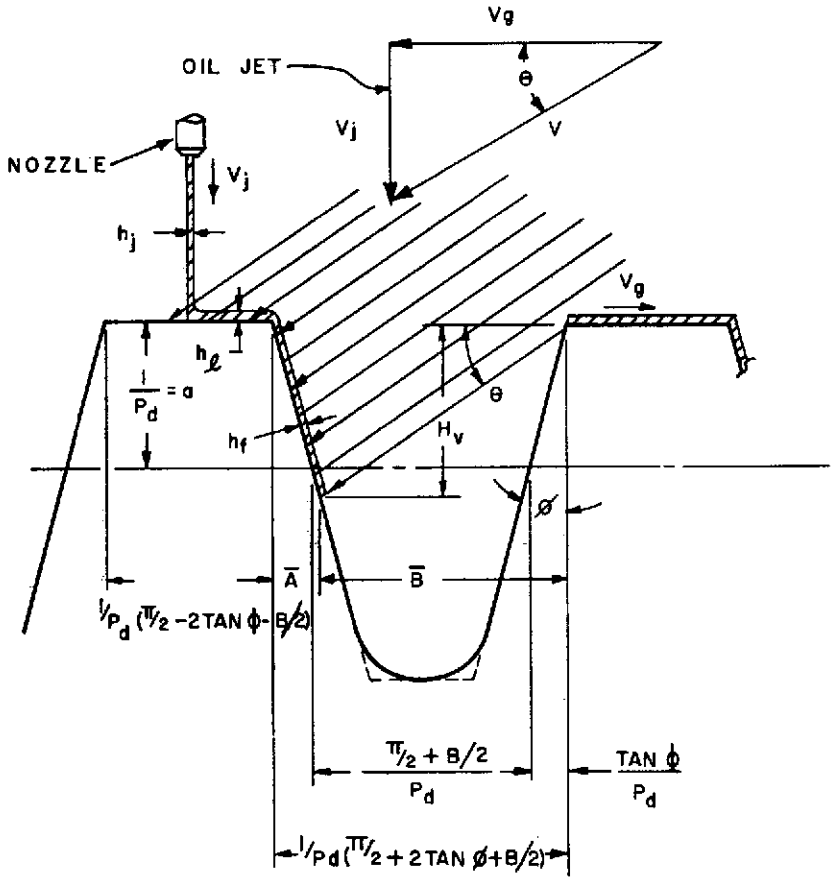

Figure 6. - Vectorial model for penetration depth.

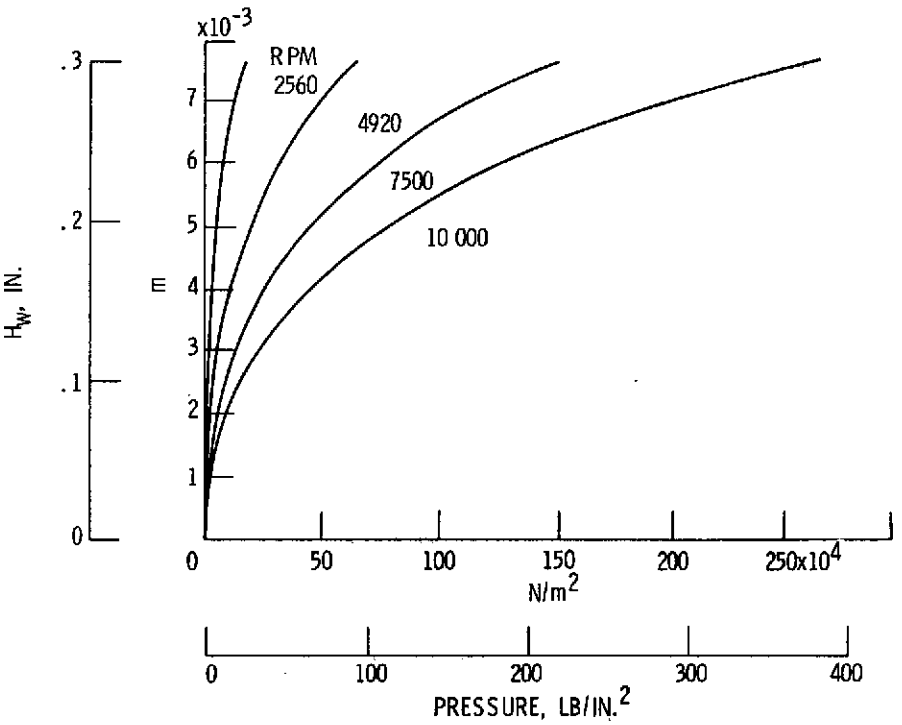

Figure 7. - Windage penetration depth as a function of oil pressure for various gear speeds. Drop size, 7.62×10^{-5} meters (.003 in.).

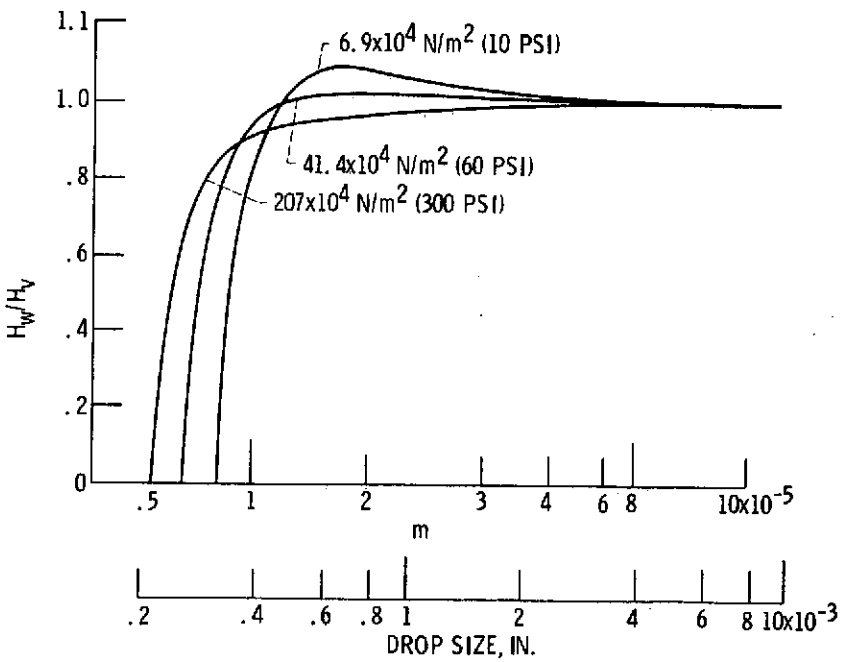

Figure 8. - Effect of drop size on windage impingement depth, 10 000 rpm.

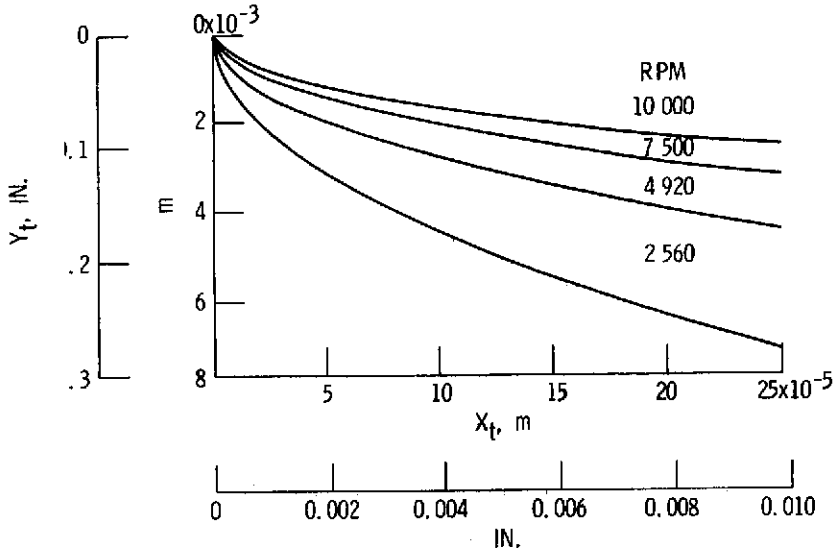

Figure 9. - Oil drop trajectory for various gear speed oil jet pressure 13.8x10^4 N/m^2 (20 psi), drop size 7.62x10^{-5} meters (0.003 in.).

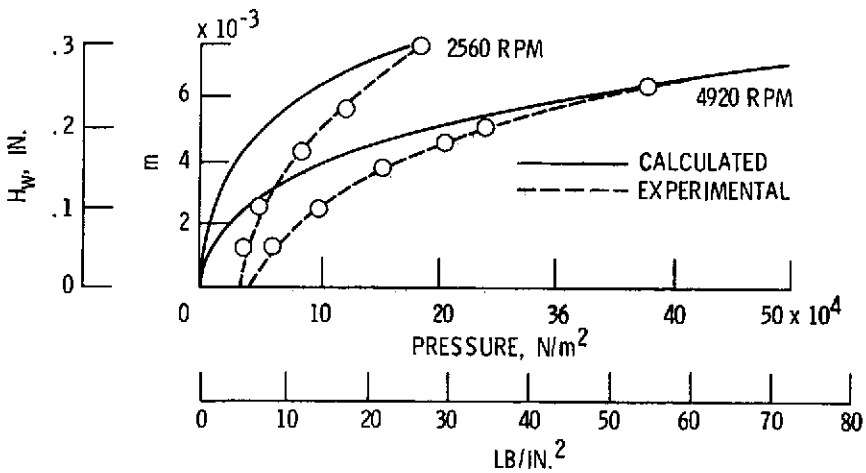

Figure 10. - Calculated and experimental impingement depth versus oil jet pressure at 4920 and 2560 rpm.

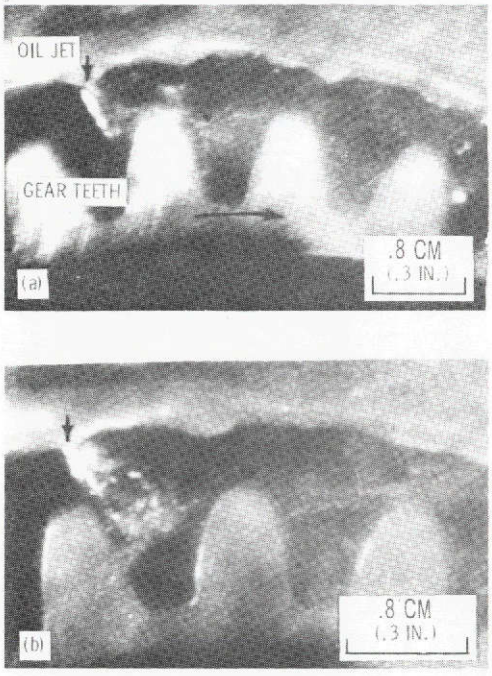

Figure 11. - Oil jet penetrating tooth space and impinging gear tooth; speed, 4920 rpm; oil pressure, 10.5×10^4 N/m^2 (15 psi); xenon and stroboscopic light.

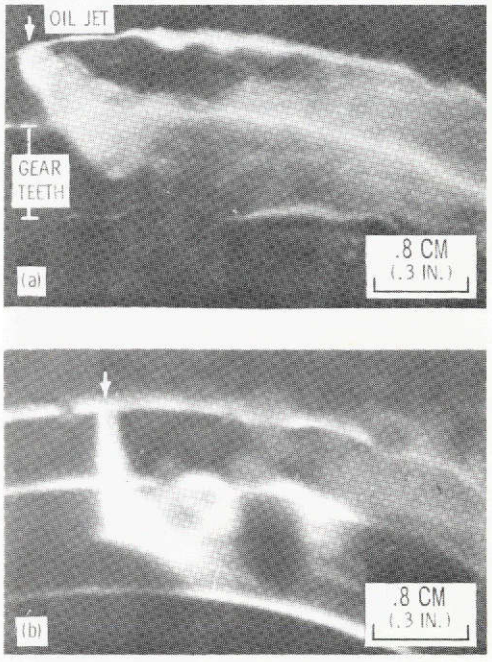

Figure 12. - Oil jet impingment and subsequent penetration; xenon light only; (a) 4920 rpm; 14×10^4 N/m^2 (20 psi); (b) 2560 rpm; 13×10^4 N/m^2 (19 psi).

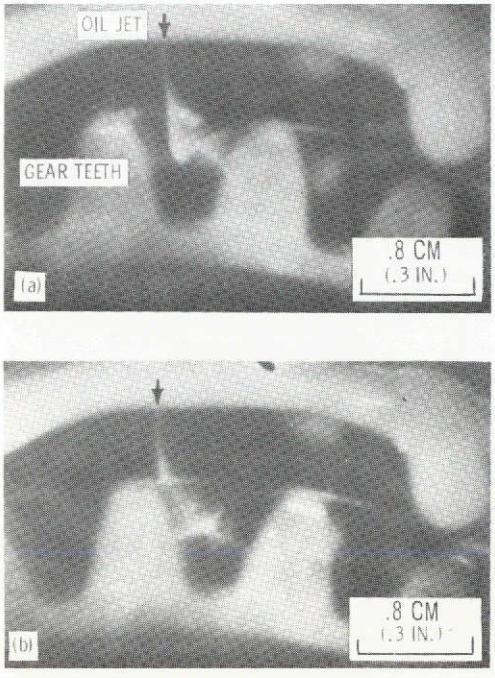

Figure 13. - Oil jet penetrating tooth space and impinging gear tooth; speed, 2560 rpm (9×10^4 N/m^2 (13 psi); xenon and stroboscopic light.

NASA-Lewis